8-21-2015

Modeling High Frequency Wave Propagation in a Three-Dimensionally Heterogeneous Earth

Steven Walsh
University of Connecticut - Storrs, steven.walsh@uconn.edu

Modeling High Frequency Wave Propagation in a Three-Dimensionally Heterogeneous Earth

Steven Walsh

B.S., University of Connecticut, 2014

A Thesis

Submitted in Partial Fulfillment of the

Requirements for the Degree of

Master of Science

At the

University of Connecticut

2015

APPROVAL PAGE

Masters of Science Thesis

Modeling High Frequency Wave Propagation in a Three-Dimensionally Heterogeneous Earth

Presented by

Steven Walsh, B.S.

Major Advisor_____

Dr. Vernon Cormier

Associate Advisor_____

Dr. Lanbo Liu

Associate Advisor_____

Dr. Michael Rozman

University of Connecticut

2015

Table of Contents

List of Figures

1. Theory

1.1 Introduction

Differences between earthquakes and explosions are largest in the highest recordable frequency band. Common seismic discriminants are based on amplitude ratios (Pg/Lg). Ideal explosions radiate only P waves, so the P/Lg ratio will be larger for explosions. We still see Lg waves from explosions due to P conversions at boundaries representing changes in velocity; particularly the crust/mantle boundary. Lg waves are multiply, critically reflected S waves trapped in the crust where the crust acts as a waveguide. Lateral variation of both small-scale heterogeneities and large scale deterministic structure can assume major control over efficiency or blockage of Lg. In the case of Lg blockage, the difference in amplitude ratios of P/Lg for earthquakes and explosions become harder to distinguish. In the highest recordable frequency band, scattering of elastic energy by small scale heterogeneity can stabilize the behavior of Lg trapped in the crust.

As frequency increases and wavelengths decrease the seismic wavefield becomes sensitive to small-scale structure including microstructure of material heterogeneity. This heterogeneity becomes a source of scattering. Modeling this small-scale structure with numerical solvers becomes increasingly difficult because of the grid fineness needed to explicitly describe it. A radiative transport method handles small-scale structure stochastically and large scale deterministically, which prevents the need for dense model meshes that explicitly describe the small-scale structure.

The goal of this paper is to describe a method for modeling high frequency seismic wave propagation via a radiative transport method in a model containing lateral variations in velocity, density, crustal thickness, and small-scale heterogeneities. Then to demonstrate the effects of these variations on regional Lg waves. Grid nodes are used to describe material properties at specified locations. Four corresponding nodes form a tetrahedron that allows for general gradients in velocity to be handled, which are important to properly model waves whose rays turn in the uppermost mantle. The tetrahedra also

provide the ability to model known lateral variations in earth structure such as crustal thickness variations like that found near ocean/continent transitions. These variations have been observed to strongly affect the arrival of Lg (Kennet, 1986).

1.2 Rays

Displacements $u(\bar{x}, t)$ of elastic media results in seismic waves due to a balance of internal stress and external forces. The homogenous equation of motion relates displacements to internal stress

$$\rho \frac{\partial^2 u_i}{\partial t^2} = \frac{\partial \sigma_{ij}}{\partial x_j} \tag{1}$$

where ρ is the density of the material and σ is the stress tensor. Helmholtz's theorem can be used to represent the displacement field as

$$\mathbf{u} = \boldsymbol{\nabla}\varphi + \boldsymbol{\nabla} \times \boldsymbol{\psi} \tag{2}$$

leading to two wave equations

$$\boldsymbol{\nabla}^2\varphi - \frac{1}{\alpha^2}\frac{\partial^2 \varphi}{\partial t^2} = 0 \tag{3}$$

$$\boldsymbol{\nabla}^2\boldsymbol{\psi} - \frac{1}{\beta^2}\frac{\partial^2 \boldsymbol{\psi}}{\partial t^2} = 0 \tag{4}$$

where $\alpha = \sqrt{(\lambda + 2\mu)/\rho}$ corresponds to the P-wave velocity and $\beta = \sqrt{\mu/\rho}$ corresponds to the S-wave velocity. By method of separation of variables we assume the three dimensional wave equation has a solution of the form

$$\varphi(x_1, x_2, x_3, t) = X(x_1)Y(x_2)Z(x_3)T(t) \tag{5}$$

which leads to a set of four coupled harmonic equations

$$\begin{aligned} &\frac{d^2T}{dt^2} + \omega^2 T = 0 \\ &\frac{d^2X}{dt^2} + k_1^2 X = 0 \\ &\frac{d^2Y}{dt^2} + k_2^2 Y = 0 \\ &\frac{d^2Z}{dt^2} + k_3^2 Z = 0 \end{aligned} \tag{6}$$

where $k_1^2 + k_2^2 + k_3^2 = \omega^2/\alpha^2$ in the case of the P wave equation. The left side of this equation being constant defines a planar surface with normal vector $\bar{k} = |\bar{k}|\hat{k} = (\omega/\alpha)\hat{k}$ called the wavenumber vector, which defines the direction of wave propagation (normal to the wavefront). This leads to the D'Alembert solution

$$\varphi(\bar{x}, t) = A(\bar{x})e^{i(\bar{k}\cdot\bar{x}-\omega t)} \tag{7}$$

Figure 1 shows a planar wavefront propagating in the x-z plane. From the figure it can be seen that the wave speed $c = ds/dt$, horizontal speed $c_x = dx/dt$, vertical $c_z = dz/dt$. The angle of incidence (measured from the vertical) can be related to the horizontal and vertical speed:

$$\sin(i) = \frac{ds}{dx} = c\frac{dt}{dx} = \frac{c}{c_x} \equiv cp \tag{8}$$

$$\cos(i) = \frac{ds}{dz} = c\frac{dt}{dz} = \frac{c}{c_z} \equiv c\eta \tag{9}$$

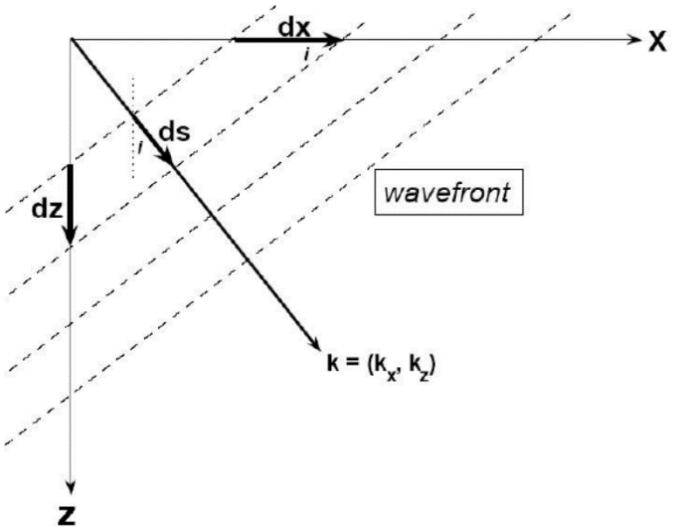

Figure 1 – A plane wave propagating in x-z plane in the **k** direction (perpendicular to the wavefront).

The first equation yields the ray parameter or horizontal slowness, and the second yields vertical slowness

$$\mathrm{p} \equiv \frac{1}{\mathrm{c_x}} = \frac{\sin(\mathrm{i})}{\mathrm{c}} \tag{10}$$

$$\eta \equiv \frac{1}{\mathrm{c_z}} = \frac{\cos(\mathrm{i})}{\mathrm{c}} \tag{11}$$

which together form the slowness vector $\bar{s} = (p, \eta)$.

Explicitly solving the equations of motion for an inhomogeneous medium can be difficult and tedious. In the high frequency spectrum, the wave motion can be approximated by studying the ray path. Consider the P-wave equation

$$\boldsymbol{\nabla}^2\varphi = \frac{1}{\alpha^2}\frac{\partial^2\varphi}{\partial \mathrm{t}^2} \tag{12}$$

with solution

$$\varphi(\bar{\mathrm{x}}, \mathrm{t}) = \mathrm{A}(\bar{\mathrm{x}})\mathrm{e}^{\mathrm{i}(\bar{\mathrm{k}}\cdot\bar{\mathrm{x}}-\omega \mathrm{t})} = \mathrm{A}(\bar{\mathrm{x}})\mathrm{e}^{-\mathrm{i}\omega \mathrm{T}(\bar{\mathrm{x}})} \tag{13}$$

where $T(\bar{x})$ represents the time required for the wavefront to reach a position $\bar{x}$. Substitution of Eq. 13 into Eq. 12 gives

$$\boldsymbol{\nabla}\varphi = \boldsymbol{\nabla}\mathrm{A}\mathrm{e}^{-\mathrm{i}\omega \mathrm{T}} - \mathrm{i}\omega \mathrm{A}\boldsymbol{\nabla}\mathrm{T}\mathrm{e}^{-\mathrm{i}\omega \mathrm{T}}$$

$$\boldsymbol{\nabla}^2\varphi = [\boldsymbol{\nabla}^2\mathrm{A} - \omega^2\mathrm{A}|\boldsymbol{\nabla}\mathrm{T}|^2 - \mathrm{i}(2\omega\boldsymbol{\nabla}\mathrm{A}\cdot\boldsymbol{\nabla}\mathrm{T} + \omega\mathrm{A}\boldsymbol{\nabla}^2\mathrm{T})]\mathrm{e}^{-\mathrm{i}\omega \mathrm{T}}$$

$$\frac{\partial^2\varphi}{\partial \mathrm{t}^2} = -\omega^2\mathrm{A}\mathrm{e}^{-\mathrm{i}\omega \mathrm{T}}$$

$$\boldsymbol{\nabla}^2\mathrm{A} - \omega^2\mathrm{A}|\boldsymbol{\nabla}\mathrm{T}|^2 - \mathrm{i}(2\omega\boldsymbol{\nabla}\mathrm{A}\cdot\boldsymbol{\nabla}\mathrm{T} + \omega\mathrm{A}\boldsymbol{\nabla}^2\mathrm{T}) = -\frac{\omega^2\mathrm{A}}{\alpha^2} = -\mathrm{A}\mathrm{k}^2 \tag{14}$$

Considering the real portion

$$\boldsymbol{\nabla}^2\mathrm{A} - \omega^2\mathrm{A}|\boldsymbol{\nabla}\mathrm{T}|^2 = -\frac{\omega^2\mathrm{A}}{\alpha^2} \tag{15}$$

and rearranging terms and dividing through by $\omega^2 A$,

$$|\boldsymbol{\nabla}\mathrm{T}|^2 - \frac{1}{\alpha^2} = -\frac{\boldsymbol{\nabla}^2\mathrm{A}}{\omega^2\mathrm{A}} \tag{16}$$

Using the high frequency approximation, the limit as $\omega \to \infty$, the right term goes to zero so

$$|\boldsymbol{\nabla}\mathrm{T}|^2 = \frac{1}{\alpha^2} \tag{17}$$

Or in general:

$$|\boldsymbol{\nabla}\mathrm{T}|^2 = \frac{1}{\mathrm{c}^2} \tag{18}$$

known as the eikonal equation which describes the kinematic propagation of high frequency waves. The eikonal equation implies

$$|\boldsymbol{\nabla}\mathrm{T}(\bar{\mathrm{x}})| = \frac{1}{\mathrm{c}(\bar{\mathrm{x}})} \tag{19}$$

$$\boldsymbol{\nabla}\mathrm{T}(\bar{\mathrm{x}}) = \frac{1}{\mathrm{c}(\bar{\mathrm{x}})}\hat{\mathrm{k}} = \bar{\mathrm{s}} = (\mathrm{p}, \eta) = \text{slowness vector} \tag{20}$$

This states that the gradient of a wavefront at position $\bar{x}$ is equal to the local slowness. The direction of maximum change of a wavefront $\left(\boldsymbol{\nabla}T(\bar{x})\right)$ defines the direction of wave propagation $\hat{k}$, where $\hat{k}$ is perpendicular to the wavefront. As c(x) changes, the direction of propagation changes (similarly if c(x) is constant than direction of propagation is straight line).

The directional cosines for a wavefront in three dimensions

$$\left(\frac{\mathrm{dx}_1}{\mathrm{ds}}\right)^2 + \left(\frac{\mathrm{dx}_2}{\mathrm{ds}}\right)^2 + \left(\frac{\mathrm{dx}_3}{\mathrm{ds}}\right)^2 = 1 \tag{21}$$

are reduced for a plane wave (Figure 1) by orienting the axes such that the wave lies in the x-z plane such that

$$\left(\frac{\mathrm{dx}}{\mathrm{ds}}\right)^2 + \left(\frac{\mathrm{dz}}{\mathrm{ds}}\right)^2 = 1 \tag{22}$$

Referring back to Eq. 20

$$\boldsymbol{\nabla}\mathrm{T}(\bar{\mathrm{x}}) = \frac{1}{\mathrm{c}(\bar{\mathrm{x}})}\hat{\mathrm{k}} = \frac{1}{\mathrm{c}(\bar{\mathrm{x}})}\left(\frac{\mathrm{dx}_\mathrm{i}}{\mathrm{ds}}\right) \tag{23}$$

and by taking the derivative with respect to ds leads to the ray path equation

$$\frac{\mathrm{d}}{\mathrm{dx_i}}\left(\frac{1}{\mathrm{c}(\bar{\mathrm{x}})}\right) = \frac{\mathrm{d}}{\mathrm{ds}}\left(\frac{1}{\mathrm{c}(\bar{\mathrm{x}})}\frac{\mathrm{dx_i}}{\mathrm{ds}}\right) \tag{24}$$

which states that the change of wavespeed is related to a change of ray geometry. Consider the case where velocity depends only on depth, $c(\bar{x}) = c(z)$:

$$\frac{\mathrm{d}}{\mathrm{ds}}\left(\frac{1}{\mathrm{c(z)}}\frac{\mathrm{dx}}{\mathrm{ds}}\right) = 0 \;\Rightarrow\; \frac{1}{\mathrm{c(z)}}\frac{\mathrm{dx}}{\mathrm{ds}} = \mathrm{const}$$

$$\Rightarrow \frac{\sin(\mathrm{i})}{\mathrm{c(z)}} = \mathrm{const} = \mathrm{p} \tag{25}$$

The angle i is called the angle of incidence, and it gives the inclination of a ray measured from the vertical. Eq. 25 is Snell's law which states that the ray parameter is constant for the entire travel path of the ray. The change in velocity correlates to a change in angle of incidence

$$\frac{\mathrm{d}}{\mathrm{ds}}\sin(\mathrm{i}) = \cos(\mathrm{i})\frac{\mathrm{di}}{\mathrm{ds}} = \frac{\mathrm{dz}}{\mathrm{ds}}\frac{\mathrm{di}}{\mathrm{ds}} = \frac{\mathrm{d}}{\mathrm{ds}}(\mathrm{pc})$$

$$\Rightarrow\; \frac{\mathrm{di}}{\mathrm{ds}} = \mathrm{p}\frac{\mathrm{dc}}{\mathrm{dz}} \tag{26}$$

such that the rate of change of incidence angle is proportional to the rate of change of velocity. In the case of no velocity fluctuations, $dc/dz = 0 = di/dz \;\rightarrow\; (i = const)$. For a constant angle of incidence the plane wave follows a straight line ray path. If velocity increases with depth the ray curves upwards and decreasing velocity results in a downward curve. There are several possible connecting ray paths which means a multiplicity of arrivals all with different initial angles and travel times. From Figure 2 an arc length along the ray path is defined as $ds = Rdi$ where R is the radius of curvature

$$\mathrm{R} = \frac{\mathrm{ds}}{\mathrm{di}} = \frac{1}{\mathrm{p}}\frac{\mathrm{dz}}{\mathrm{dc}} = \frac{1}{\mathrm{p}(\frac{\mathrm{dc}}{\mathrm{dz}})} \tag{27}$$

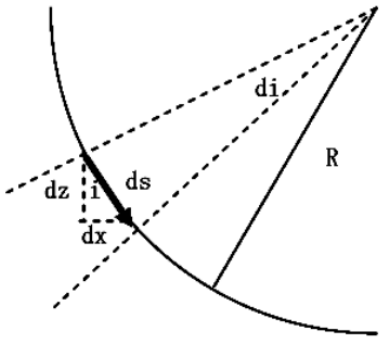

Figure 2 – Ray path determined by radius of curvature (Van Der Hilst, 2008).

The ray travels along a path determined by the radius of curvature unless interrupted at a boundary representing a change in velocity. Consider the simple two layer scenario of an incident ray striking a boundary separating acoustic media of velocities c_1 and c_2. The energy of the incident ray is partitioned between a reflected and refracted ray. The two excited rays share the same ray parameter as the incident ray which determines the angle of inclination via Snell's law:

$$\frac{\sin(\mathrm{i})}{\mathrm{c}_1} = \frac{\sin(\tau)}{\mathrm{c}_2} = \mathrm{p} \tag{28}$$

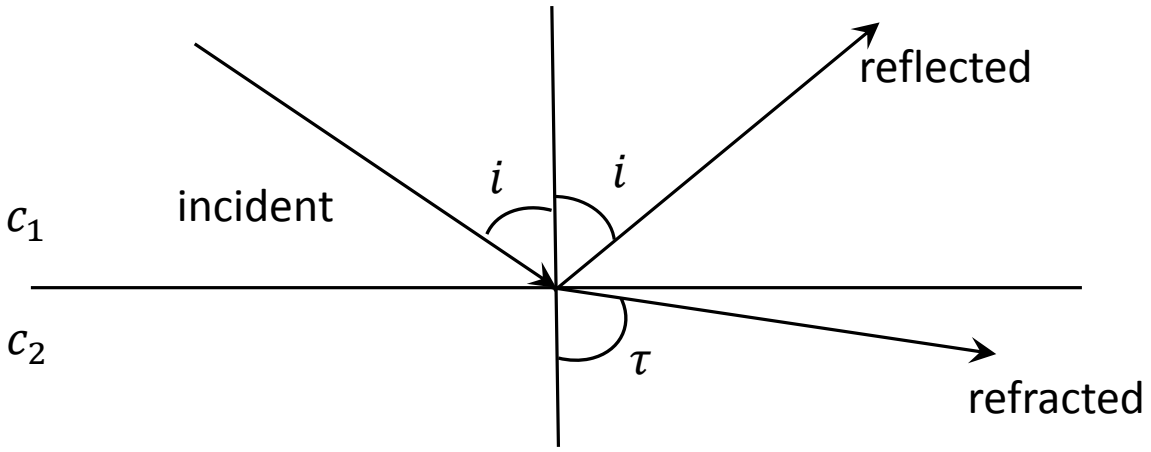

Figure 3 – Incident ray striking a boundary separating acoustic media of different velocities.

As τ approaches 90° (Figure 3), Snell's law predicts a critical refraction

$$\frac{\sin(\mathrm{i_c})}{\mathrm{c_1}} = \frac{\sin(90°)}{\mathrm{c_2}} = \frac{1}{\mathrm{c_2}} \tag{29}$$

which results in a refracted wave traveling horizontally directly below the interface known as a head wave. A head wave continuously transmits energy back into the previous layer as it travels along the interface, at the same critical angle

$$\mathrm{i_c} = \sin^{-1}(\mathrm{c_1}/\mathrm{c_2}) \tag{30}$$

If $i > i_c$ sometimes label postcritical, no seismic energy can penetrate the boundary and thus all energy is reflected. If $c_2 < c_1$, no critical angle exists and the ray is deflected toward the vertical. If $c_2 > c_1$, three primary travel paths exist between source and receiver: the direct arrival, a reflected arrival, and a head wave.

For an elastic medium there exists both compressional waves (P) and shear waves (S). Particle motion of P waves is in the direction of motion and causes a change in medium density. An SV wave is an S wave polarized in the plane defined by the normal to the interface and the incident ray. An SH is an S wave polarized perpendicular to the SV plane.

When a P or SV wave impinges on a boundary four excited waves result: the transmitted P′, the transmitted SV′, the reflected P, and the reflected SV (Figure 4). By Snell's law each ray shares the incident wave's ray parameter p such that:

$$\frac{\sin(\mathrm{i})}{\alpha_1} = \frac{\sin(\tau)}{\beta_1} = \frac{\sin(\tau')}{\beta_2} = \frac{\sin(\mathrm{i}')}{\alpha_2} = \mathrm{p} \tag{31}$$

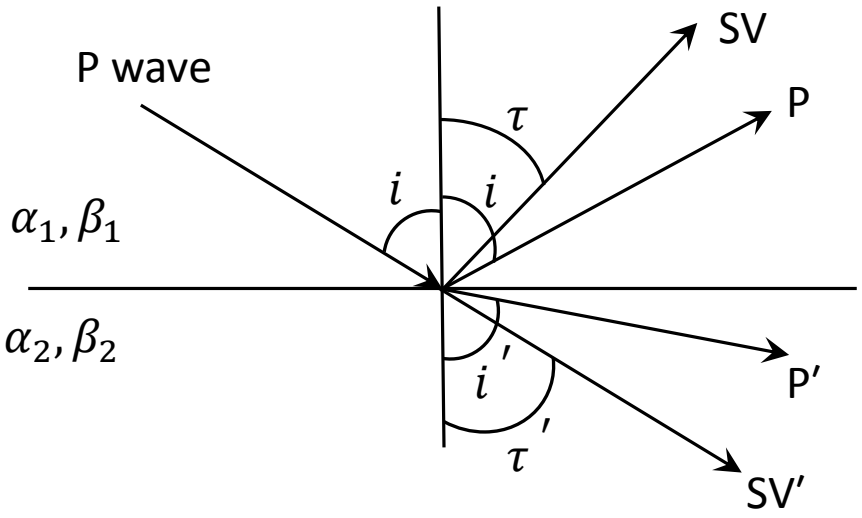

Figure 4 – Incident P wave striking a boundary of varying velocity between two elastic media.

When an SH wave encounters a discontinuity only two waves are excited (SH reflected and SH transmitted). Snell's law predicts the geometry of wave interactions but not the amplitudes. Reflection and transmission coefficients are needed to determine amplitude partitioning.

As an elastic wave propagates through the earth the energy of the wave dissipates through various processes. There are three main sources of energy attenuation along the ray path: geometric spreading, intrinsic attenuation, and scattering. In a homogeneous layer, wave amplitude decays with distance ~ 1/R known as geometric spreading. In the case of a perfectly elastic earth, geometric spreading and the reflection/transmission of energy at boundaries of varying velocity control the amplitude of a seismic wave. Attenuation through nonelastic processes designated as internal friction are parameterized with a quality factor Q. Inverse Q is known as intrinsic attenuation such that large values of Q correspond to small attenuation. The amplitude decay due to intrinsic attenuation as a function of distance can be expressed as

$$A(\bar{x}) = A_0 e^{-(\frac{\pi f}{Qv})\bar{x}} = A_0 e^{-(\frac{\pi t f}{Q})} \tag{32}$$

The final source of amplitude loss is a result of scattering caused by a wavefield's interaction with small-scale heterogeneities. As the frequency increases and wavelength decreases, the propagating

wave becomes more susceptible to these small-scale heterogeneities. These heterogeneities act as secondary sources (Huygens' principal), reradiating the incident energy by different amounts and in different directions with possible mode conversions between P and S.

1.3 Radiative Transport

Radiative transport is a particle method of forward modeling for high frequency waves using a combination of ray theory and scattering theory. A major advantage over numerical wave equation solvers in high frequency simulations is no requirement for a high-density grid to explicitly describe small-scale structure. This is achieved by handling scattering due to small-scale structure in a stochastic manner. Some other key advantages of this Monte Carlo particle based approach: energy conservation guaranteed, single and multiple scattering naturally generated, intrinsic attenuation easily modeled, P and S waves can be modeled separately. Intrinsic attenuation included by reducing energy contained in each particle as a function of travel time, Eq. 32.

A point source at a fixed location and time emits packets of elastic energy with a given direction determined by the source radiation pattern. Each packet of elastic energy, which we refer to as a phonon (Shearer, 2004), follows a deterministic ray path until affected by a discontinuity or scatterer. At a discontinuity, reflection and transmission coefficients are treated as probabilities that determine the new direction and possible mode conversion of a phonon. Scattering is treated in a similar fashion.

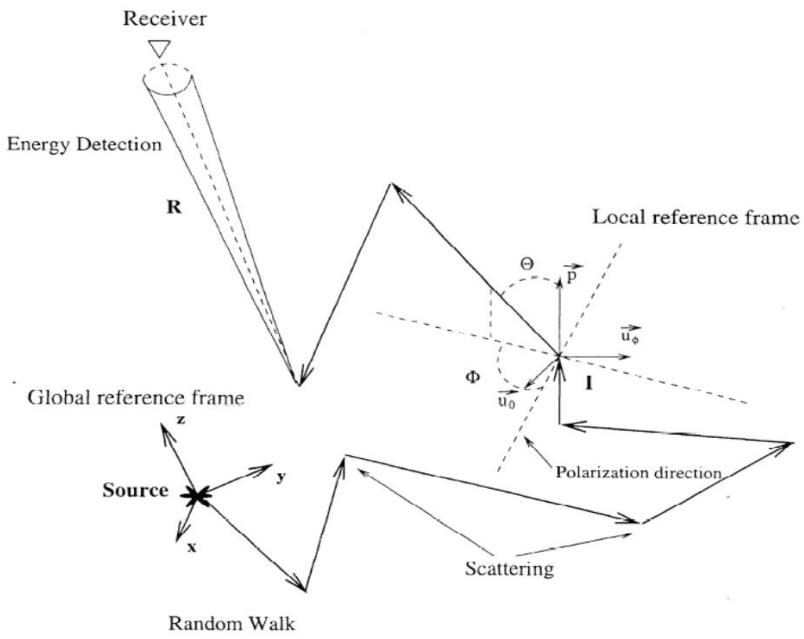

Figure 5 – Radiative transport schematic showing the propagation of elastic energy from source to receiver. Scattering due to small-scale heterogeneities redirects the energy (Cormier, 2014).

1.4 3D Model

A phonon's path through the model is determined through a combination of ray theory, for deterministic propagation through background (large-scale) structure, and through scattering theory for stochastic handling of scattering due to small-scale heterogeneities. Large-scale structure is defined as $ka \gg 1$ and small-scale structure $ka \sim 1$, where a is the typical feature size and k is the wavenumber corresponding to wavelength.

The large-scale structure is modeled via tetrahedral cells, each constructed using four grid nodes. These nodes define attributes of the model at set locations (velocity, density, Q). Using the node positions and attributes, linear gradients can be computed for each tetrahedron. Five tetrahedra combine to form a basic building block (Figure 17), constructed using eight grid nodes (see Model Construction section). These blocks are then stacked in three dimensions to construct the deterministic model (Figure 6 left). The small-scale structure is a perturbation to the deterministic structure (Figure 6 right).

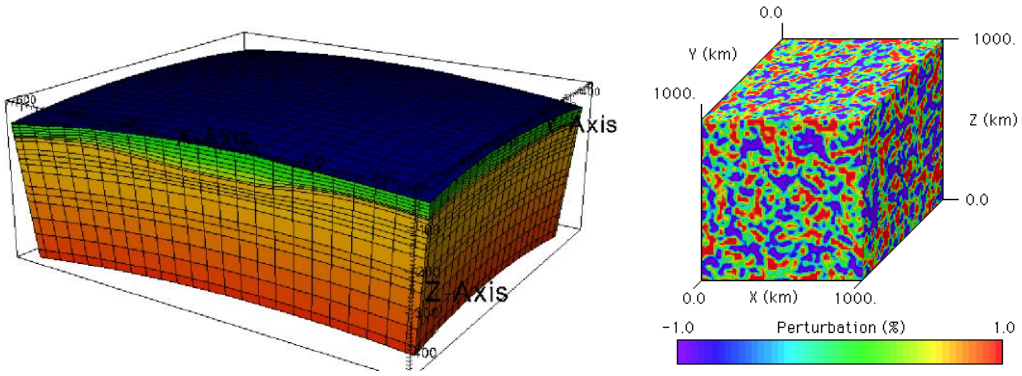

Figure 6 – Model containing large-scale deterministic structure (left), with statistical structure (right) as a perturbation.

1.5 Deterministic Ray theory in a Tetrahedral Model Cell

Recall linear velocity gradients in the earth results in circular ray paths. Referring back to Eq. 27, if c varies smoothly then $dc/dz = const$ which implies the radius of curvature R is constant. We model linear gradients via tetrahedral model cells, so while a phonon propagates in the cell it follows a circular path.

The next section follows closely with (Menke, 2002). A tetrahedral model cell made up of four nodes has a linear velocity gradient **g**. A ray with starting point $\mathbf{x_0}$ and ray tangent **t** is thus confined to the t-g plane as shown in Figure 7. This geometry is best analyzed in a rotated coordinate system (**x**',**y**',**z**') in which the ray propagates in the **x**'-**z**' direction where **z**' is parallel to **g** and **x**' increases with **t**. This situation is equivalent to a ray propagating in a medium with a linear velocity in **z**'. A ray in such medium is known to have a radius of curvature R = 1/(s|**g**|) where s is the horizontal slowness in the **x**' direction ($\mathbf{t}_{x'}/\ \mathbf{v}(\mathbf{x_0})$). The center of the circle is a distance R from $\mathbf{x_0}$ in a direction perpendicular to **t** ($\mathbf{x_0}$' + $R\mathbf{t}_{z'}$, $\mathbf{y}_{0'}$, $\mathbf{z}_{0'} - R\mathbf{t}_{x'}$) which typically lies outside of the tetrahedron Figure 7. No physical ray should ever cross the **z**' = 0 level as the resulting velocity is less than or equal to zero.

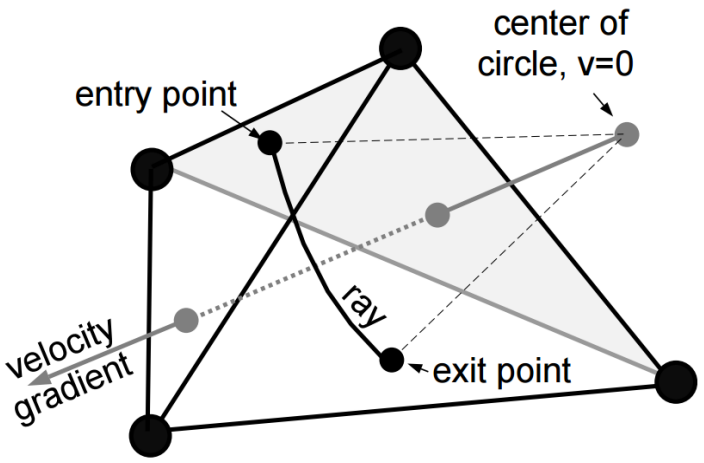

Figure 7 – Ray propagation through a tetrahedron with linear velocity gradient results in circular path defined by a constant radius of curvature (Menke, 2004).

The procedure then is to perform a coordinate transformation to the prime coordinate system which involves both rotation and translation. In the new system, **x**' is parallel to increasing **t** ((gxt)xg), **z**' is parallel to **g**, and **y**' is the axis without motion (gxt). The transformation matrix **S** from world space to a rotated system is comprised of unit vectors parallel to gxtxg, gxt, g. The rotated system is then shifted such that the center of the circle defined by the radius of curvature is at the origin. The rotated and translated system is designated the prime system. Any point **x** in world space can be transformed to the prime system by $\mathbf{x}' = \mathbf{S}\mathbf{x} - \mathbf{x}_{c'}$, and inversely transformed $\mathbf{x} = \mathbf{S}^{\mathbf{T}} (\mathbf{x}' + \mathbf{x}_{c'})$.

In order to determine the exit face of the tetrahedron, an intersection with the cellface and ray path must occur. In the prime system a face has an equation of a plane ax'+by'+z'+d' = 0. As the ray lies in the plane of y'=0, the intersection point of the ray with the face is equivalent to finding the intersection point of the line ax'+cz'+d'=0 with a circle of radius R centered at the origin Figure 8.A. Suppose we construct a second line that passes through the origin and which is the perpendicular bisector of the first. The bisector has an equation –cx'+az'=0 and intersection point

$$(x', z') = \frac{-d}{(a^2 + c^2)} (a, c) \tag{33}$$

which is a distance

$$D = \frac{|d|}{(a^2 + c^2)} \tag{34}$$

from the origin. The bisector **b** points in the direction **b** = [sin(β) , cos(β)]. The angle to this bisector β can be found using the relationship

$$\sin(\beta) = \frac{-da}{(a^2 + c^2)} \tag{35}$$

$$\cos(\beta) = \frac{-dc}{(a^2 + c^2)} \tag{36}$$

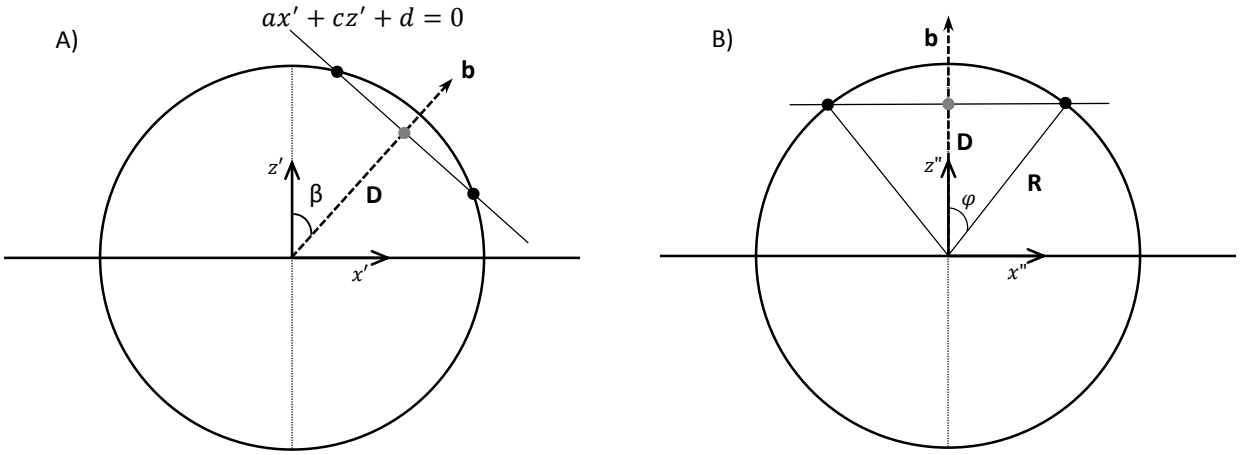

Figure 8 – Prime system (left) in which z' is parallel to the velocity gradient. Rotated prime system (right) in which z'' is parallel to the bisector which is perpendicular to the line representing a cellface.

Rotating the prime system in Figure 8.A by β such that the bisector points in the z'' we can see there is mirror symmetry about this axis (Figure 8.B). The intersections points of the cellface with the ray path are at angles φ = acos(D/R) and – φ. The angle to each intersection in the prime coordinate system is then θ = β ± φ. Recall that the ray had a starting point $\mathbf{x_0}$ corresponding to an azimuthal angle in the prime system θ_0. For each intersection of each face we calculate $\theta - \theta_0$ to find the smallest positive value, which determines the exit location.

2. Implementation

2.1 Media Objects

Cellface – The cellface object stores the attributes of each face (most importantly its spatial orientation and outward normal). It is constructed using four nodes where the first three define the surface and the fourth is used to determine the direction of the normal. For tetrahedral model cells, the cellface normal points outward away from the center.

Consider the figure below. First we construct rays PQ and PR, then take their cross product to obtain a normal to the face. Next we take the dot product of the normal with ray PS. If the dot product is positive then the normal is pointing inward and must have its direction negated.

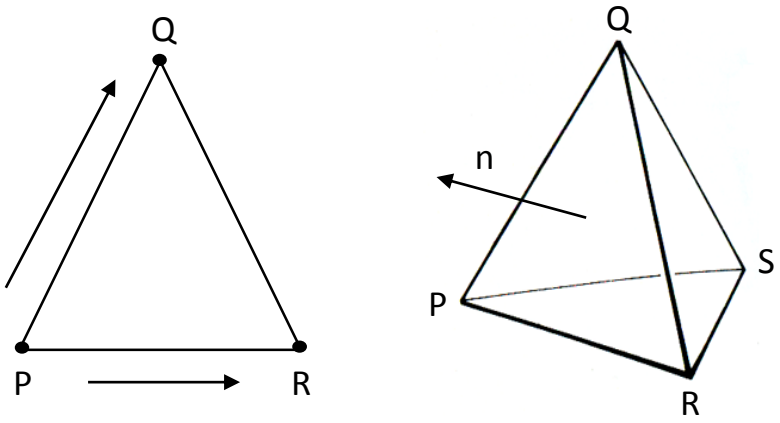

Figure 9 – Cellface (left), tetrahedron consisting of four faces (right). Normal of cellface n determined by $PQ \times PR$. If $PS \times n \geq 0$ normal is pointing inward and must be negated.

In regards to deterministic ray tracing, it is simpler to store only one point $\mathbf{x_o} = (x_0,y_0,z_0)$ for each cellface and its outward normal $\mathbf{n} = [a,b,c]$. This gives an equation for the cellface

$$ax + by + c + d = 0 \tag{37}$$

$$d = -ax_0 - by_0 - cz_0 \tag{38}$$

Tetrahedral model cell – A tetrahedral model cell is defined using four points in space and their associated attributes such as velocity, density, ect. Using these four nodes, four cellfaces are constructed and linear gradients are computed. Given each node position x_i , i= 1,…4 and corresponding velocity v_i, i = 1,…4 the velocity as a function of position is defined as

$$v(x) = a_1 x + a_2 y + a_3 z + a_4 \tag{39}$$

The 4-vector of coefficients **a** = $[a_1, a_2, a_3, a_4]^T$ can be found solving the 4x4 linear system:

$$v_i(x) = a_1 x_i + a_2 y_i + a_3 z_i + a_4 \; ; \quad i = 1, \ldots 4 \tag{40}$$

Or

$$V = M \text{ dot } a \tag{41}$$

where **V** is a 4-vector of nodal velocities and **M** is a 4x4 matrix containing node positions (with the fourth column consisting of unity). The velocity gradient is the 3-vector **g** = $[a_1, a_2, a_3]^T$ and a_4 is the velocity at $v(0)$. We solve this 4x4 linear system using Gaussian elimination as matrix inversion involves more computation. This method can be used for any linear gradient within the tetrahedral. Once the coefficients have been solved, the velocity can be computed at any location within the tetrahedral.

Another important function of the tetrahedral model cell is the knowledge of whether a given location is inside the cell. A location is only considered inside the cell if it is inside with respect to all four faces. The procedure is similar to determining the direction of the outward normal for each face. Each cellface is described by a point and a normal to the plane. A ray is constructed from the cellface point to the location in question, then dotted with the cell face normal. A value less than or equal to zero shows the point as inside with respect to that face. By performing this operation for each face and analyzing the largest value it can be determined whether a given point lies within the cell.

2.2 Simplistic Overview of Radiative Transport through Tetrahedral Model Cell

Given grid nodes with spatial orientations and physical properties at those locations, construct a model comprised of tetrahedral cells. The tetrahedra handle the process of calculating gradients from nodes as well as deterministic ray tracing.

The source (described by a moment tensor) emits phonons (packets of elastic energy) based on the source radiation pattern. These phonons contain information regarding their current position, direction, ray type, and energy. Each phonon propagates through the model using deterministic ray tracing with scattering as a perturbation field. This means the phonon follows a deterministic path until a scattering event occurs.

First we calculate the deterministic arc length to each of the tetrahedron's faces and its corresponding exit location, taking the shortest positive arc length as the correct exit. Then randomly generate a scattering length and compare against the arc length to exit. If the scattering length is shorter than the arc length to exit, then the phonon scatters. The process continues until the individual phonon is collected in a bin, terminated via exiting the model at some point other than the surface, or times out.

2.3 Complete Description of Functions

2.3.1 CoordinateTransformation

Ray theory states that the motion of a ray is confined to the **t**-**g** plane where **t** is the ray tangent and **g** is the linear velocity gradient. This motion is best analyzed in a transformed coordinate system in which the ray propagates only in the **x**'-**z**' directions (where **z**' is parallel to **g** and **x**' increases with **t**). This is equivalent to a ray propagating in a medium with a linear velocity in **z**'. A ray in such medium is known to have a path that is exactly an arc of a circle with a radius of curvature $R = 1/s|\mathbf{g}|$, where s is the

horizontal slowness in the **x**' direction ($\mathbf{t}_{x'}/\ \mathbf{v}(\mathbf{x}_0)$). The center of the circle is located at ($\mathbf{x}_{0'} + R\mathbf{t}_{z'}$, $\mathbf{y}_{0'}$, $\mathbf{z}_{0'} - R\mathbf{t}_{x'}$), where $\mathbf{t}_{z'} = \mathbf{t}$ dot $\mathbf{v}_3$ and $\mathbf{t}_{x'} = \mathbf{t}$ dot $\mathbf{v}_1$.

The rotation matrix **S** is used to transform the world space coordinates into the new prime coordinate system. **S** consists of three vectors parallel to **x**', **y**', **z**' computed as follows:

$$\mathbf{v_1} = (\mathbf{g} \times \mathbf{t}) \times \mathbf{g}$$

$$\mathbf{v_2} = (\mathbf{g} \times \mathbf{t})$$

$$\mathbf{v_3} = \mathbf{g}$$

$$\mathbf{S} = [\mathbf{v_1} \quad \mathbf{v_2} \quad \mathbf{v_3}]^{\mathrm{T}} \tag{42}$$

Applying both the coordinate rotation matrix **S** as well as the origin shift $\mathbf{x}_{c'}$ any location in world space can be transformed to the prime coordinate system $\mathbf{x}' = \mathbf{S}\mathbf{x} - \mathbf{x}_{c'}$. The inverse transformation $\mathbf{x} = \mathbf{S}^{\mathrm{T}}(\mathbf{x}' + \mathbf{x}_{c'})$.

The CoordinateTransformation object takes the velocity at current location $\mathbf{v}(\mathbf{x}_0)$, velocity gradient **g**, phonon's current location $\mathbf{x}_0$, and ray tangent **t** and computes four objects necessary for all calculations in the primed system: the current location in the new primed system $\mathbf{x}_{0'}$, origin shift $\mathbf{x}_{c'}$, transformation matrix **S**, and radius of curvature R.

$$\mathbf{x}_0' = S\boldsymbol{x}_0 - \boldsymbol{x}_c' \tag{43}$$

$$\boldsymbol{x}_c' = (\mathrm{R}t_z', 0, -\mathrm{R}t_x') \tag{44}$$

$$\mathbf{S} = \begin{bmatrix} (\mathbf{g} \times \mathbf{t}) \times \mathbf{g} \\ (\mathbf{g} \times \mathbf{t}) \\ \mathbf{g} \end{bmatrix} \tag{45}$$

$$\mathrm{R} = \frac{\mathrm{v}(\mathrm{x}_0)}{\mathrm{t}_x' \cdot |\mathbf{g}|} \tag{46}$$

2.3.2 GetCircArcDistToFace (GCAD)

Computes arc length and exit position for a particular face given the radius of curvature R, rotation matrix **S**, and origin shift $\mathbf{x}_{c'}$. This information is returned as a RetVal object (covered in the next section) which contains angles to the cellface exit, entry, and bisector.

A cellface is essentially an infinite plane defined by a point (x_0,y_0,z_0) and a normal to the surface **n**=[a,b,c] with an equation: $ax + by + c + d = 0$ where $d = -ax_0 - by_0 - cz_0$. The equation must be transformed to the prime system to test for intersection points with the ray path. Applying the rotation matrix **S**, origin shift $\mathbf{x}_{c'}$, and noting we are dealing with the 2-D x'-z' system, the new equation for the cellface becomes

$$a'x' + c'z' + d' = 0 \tag{47}$$

$$d' = -a'x'_0 - b'y'_0 - c'z'_0 \tag{48}$$

Note although we are dealing with the y=0 plane, y'_0 is not necessarily zero. Referring back to Figure 8, the angle to bisector which intersects the line of the cellface is given as

$$\beta = \text{atan2}(a', c') \tag{49}$$

and is a distance

$$|D| = \left| \frac{-d}{(a'^2 + c'^2)} \right| \tag{50}$$

from the origin.

In the case of |D| > R, no intersections with the ray path exist indicating that along this particular path the ray shall never exit the tetrahedron via this particular face. This is represented by entry and exit values of ± infinity.

In the case of |D| < R the angle to each intersection is computed. There are three scenarios to consider: β <= -90, β >= 90, -90 < β < 90. The angle to entry and exit can thus be explicitly defined as β

± φ where φ is the angle to intersection in the double prime system φ = acos(D/R) (see Ray Theory section). Each scenario is depicted below:

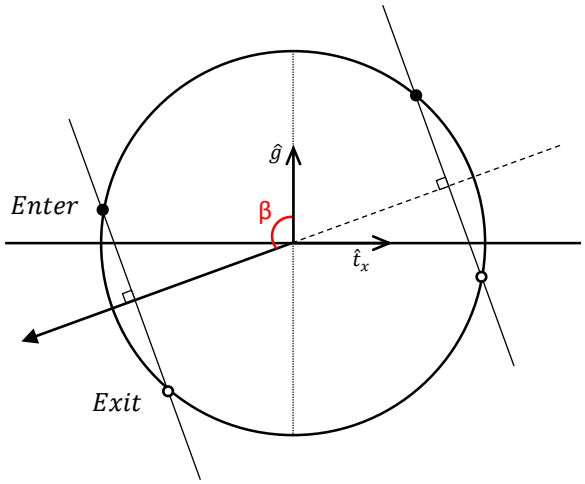

• ***When β satisfies: β <= -90°***

	Value	Promote if:	Promote To:
mEnter	β + φ	>= +90; <= -90	+inf; -inf
mExit	β - φ + 360	>= +90	+inf
mHalf	+inf		
mContinuous	true		

Figure 10 – Scenario of angle to bisector less than -90 degrees with corresponding return values.

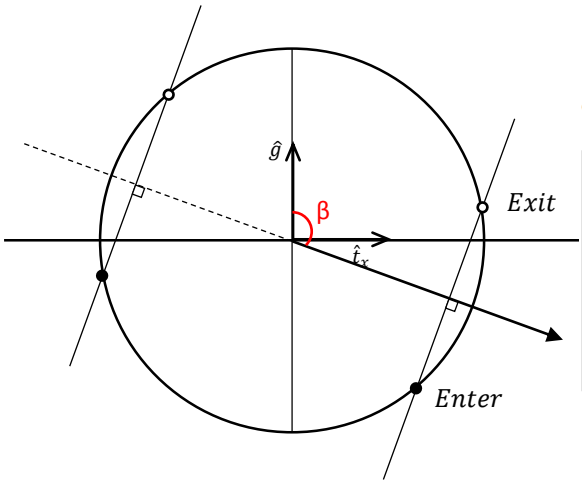

• ***When β satisfies: β >= +90°***

	Value	Promote if:	Promote To:
mEnter	β + φ - 360	<= -90	-inf
mExit	β - φ	>= +90; <= -90	+inf; -inf
mHalf	+inf		
mContinuous	true		

Figure 11 – Scenario of angle to bisector greater than -90 degrees with corresponding return values.

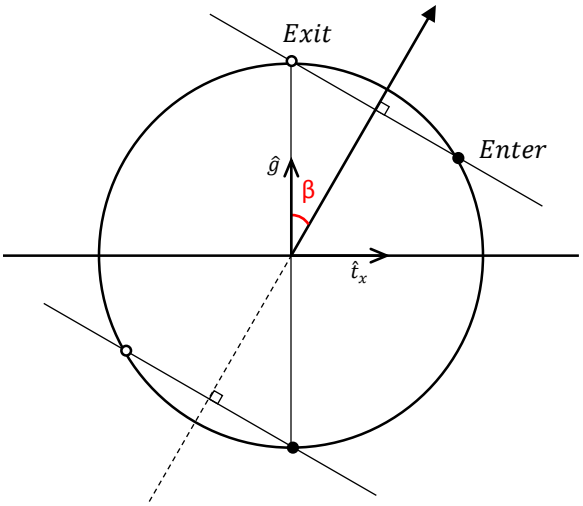

• ***When β satisfies: -90° < β < +90***

	Value	Promote if:	Promote To:
mEnter	β + φ	>= 90	+inf
mExit	β - φ	<= -90	-inf
mHalf	β		
mContinuous	false		

Figure 12 – Scenario: -90 < beta < 90 with corresponding return values.

2.3.3 GCAD_RetVal

Return value class for GCAD function which contains the angle to entry, exit, and bisector in the prime system. It encapsulates several member functions to ensure the correct exit is selected in the event of numerical error or incorrect modeling by the user.

Proper exit algorithm: In the event of numerical error it is possible that the phonon will be placed just outside of a cell (exiting or entering). Careful handling must be taken to ensure proper transfer between tetra cells; our solution is the proper exit algorithm.

Proper phonon propagation in the prime system is between -90 to 90 degrees. The other two regions (between -90 to -180, and 90 to 180) correspond to a negative phonon velocity. Constraining proper propagation further, the phonon must also be "inside" with respect to each cellface. If we consider the intersection point of the bisector with a cellface (Eq. 33) as the origin and construct a ray from that origin to the phonon's position, then dot that with the cellface normal we can determine whether the

phonon is "inside" with respect to the cellface Figure 13. A value greater than zero indicates outside, less than zero indicates inside, and equal to zero indicates on the face surface.

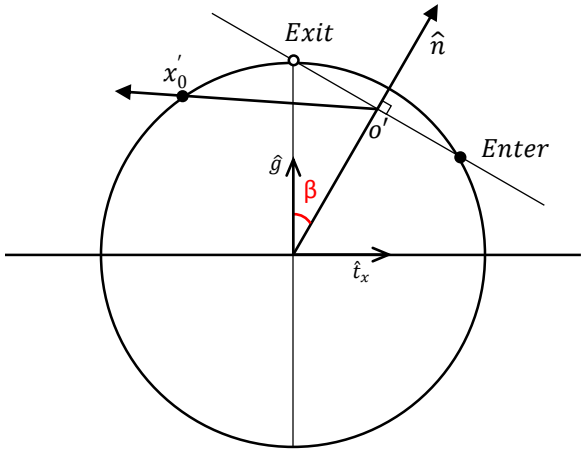

Figure 13 – Test to determine whether phonon is inside with respect to a particular cell face. If $o'x_0' \cdot n \leq 0$, where o' is the bisector point Eq. 33, then the phonon is inside.

This is a conceptual test and not actually implemented, however knowing this there are only two cases to consider: one in which the ray path is continuous and one in which it is not. By this we mean along the ray path (-90 to 90) the phonon is either always inside (continuous) or at some point along the path exits and reenters with respect to that face (not continuous). As an example, Figure 13 is a case where the ray path is not continuous. Any phonon propagation in the region between the exit and entry intersection points is "outside" with respect to the cellface and thus not proper. Using this concept we can construct a map of proper propagation regions seen below.

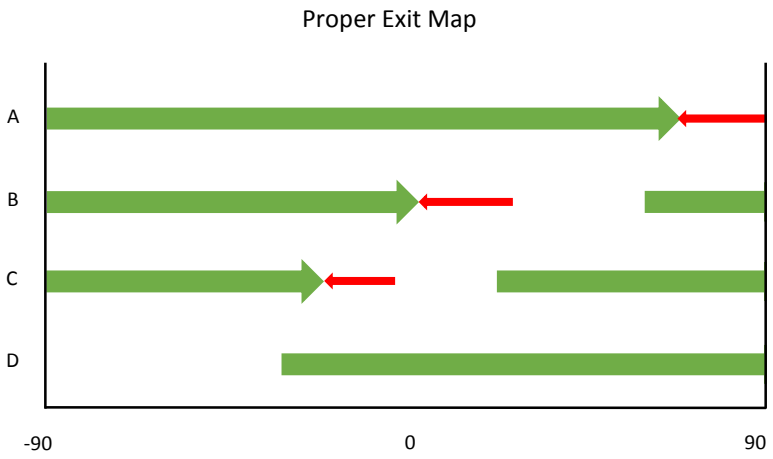

Figure 14 – Proper exit map showing regions of proper phonon propagation (green). An exit (point of arrow) is proper if it lies in the proper propagation region of all other faces; In this case, faces A and C are proper exits.

The green region indicates proper propagation of the phonon with respect to that particular face (it is inside the face and in the range of -90 to 90). The exit position lies at the endpoint of the green arrows. An exit is considered proper if it lies within the proper propagation region of all the other faces. The red region beyond the exits are considered 'back travel' regions where the phonon lies just beyond the cellface exit. In the event of numerical error where a phonon resides in a back travel region and that region is determined to be the proper exit, the arclength for the phonon (and consequently its travel time) are negative. This ensures proper handling of cell to cell transitions as the coordinate transform as well as gradients are determined by the tetrahedron in which the phonon resides. Below are two examples of phonon positions and how the proper exit algorithm handles them.

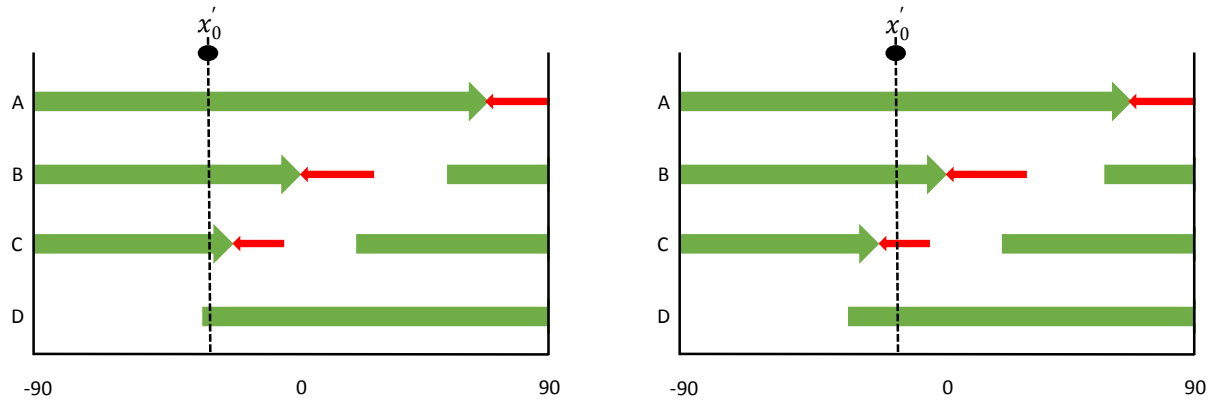

Figure 15 – Two scenarios are shown. The first illustrates an ideal situation where the phonon travels forward travel to face C (left). The second illustrates a back travel scenario to face C (right).

In both scenarios, face A and face C are both considered proper exits (as they are 'inside' with respect to all other faces). In scenario A, face C will be chosen as it is the closest proper exit. For scenario B, face C is also chosen as the phonon's position **xo'** lies in the back travel region of a proper exit. Scenario B is a case where the phonon has been placed outside of the cell via numerical error and should back travel to the surface of the cellface. Had we not allowed for back travel due to numerical error, face A would have been chosen. This would result in the phonon traveling along an incorrect ray path. The first scenario is the ideal case when the phonon is in the green region (inside with respect to each face) and thus travels to the shortest positive arc length to an exit.

2.3.4 GetPathToBoundary

Given a phonon with direction **t** and location $\mathbf{x_0}$, this highest level function which uses the tools previously discussed to determine the path length to the tetrahedral cell boundary. Using information from the phonon and the tetrahedral cell (direction, location, velocity gradient, velocity at current location) we calculate the radius of curvature, rotation matrix, origin shift, and prime location of the phonon via the CoordinateTransformation function. A return value object containing the angle to entry, exit, and midpoint for each of the four faces is constructed using the GetCircArcDistToFace function. Then we compare each exit to the green propagation region (region between -90 and 90 in which the ray

path is 'inside' with respect to the cellface) to determine whether it's a proper exit. The smallest (potentially negative) arc length out of the list of proper exits determines the selected exit and corresponding cellface.

2.3.5 AdvanceLength

Computes the new location and direction in world space for a phonon through a tetrahedron assuming the path length is known in advance. In the prime system the arc length traveled corresponds to angle θ = arclength/R, where the radius of curvature is divined by the coordinate transformation function. This angle θ defines the angle between the phonon's current position $\mathbf{x_0}$' with azimuthal angle ψ= atan2($x_{0'}$,$z_{0'}$) and its new position after propagation **x'** with azimuthal angle ψ+ θ Figure 16. To ascertain the x and z coordinates of **x'** we rotate to a new double-prime system by an angle ψ + θ/2 such that the azimuthal angle to $\mathbf{x_0}$" and **x**" is ± φ (where φ has a magnitude of θ/2. It can be easily seen that the coordinates of **x**" = (Rsin(θ /2), Rcos(θ /2)).

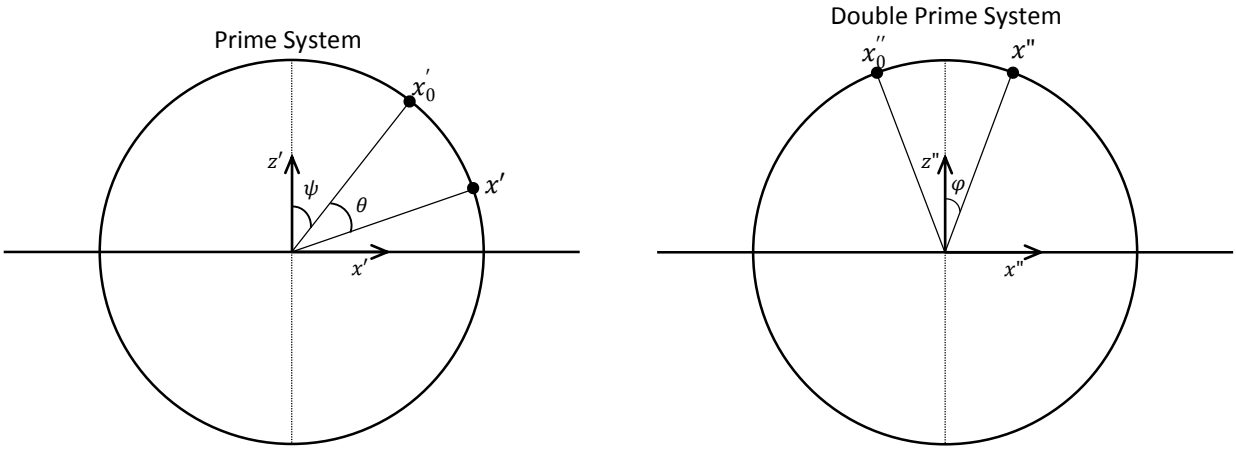

Figure 16 – Rotation of prime system to double prime system to calculate angle to exit.

Applying the rotation matrix

$$\begin{bmatrix} \cos\left(\psi+\frac{\theta}{2}\right) & \sin\left(\psi+\frac{\theta}{2}\right) \\ -\sin\left(\psi+\frac{\theta}{2}\right) & \cos\left(\psi+\frac{\theta}{2}\right) \end{bmatrix} \tag{51}$$

to **x**" we obtain the new position coordinates in the prime system:

$$x' = \cos\left(\psi+\frac{\theta}{2}\right)\cdot \mathrm{R}\sin\left(\frac{\theta}{2}\right) + \sin\left(\psi+\frac{\theta}{2}\right)\cdot \mathrm{R}\cos\left(\frac{\theta}{2}\right) \tag{52}$$

$$z' = -\sin\left(\psi+\frac{\theta}{2}\right)\cdot \mathrm{R}\sin\left(\frac{\theta}{2}\right) + \cos\left(\psi+\frac{\theta}{2}\right)\cdot \mathrm{R}\cos\left(\frac{\theta}{2}\right) \tag{53}$$

Recall the transformation to the prime system $\mathbf{x}' = \mathbf{S}\mathbf{x} - \mathbf{x}_{c'}$. Transforming the new location in the prime system to world space requires the inverse transformation $\mathbf{x} = \mathbf{S}^{\mathbf{T}}(\mathbf{x}' + \mathbf{x}_{c'})$.

Determining the new direction requires finding the ray tangent at the new location in the prime system (in the clockwise direction). This yields a new direction

$$\mathbf{t}' = [\cos(\psi+\theta), -\sin(\psi+\theta)] \tag{54}$$

Applying the inverse transformation yields the new direction in world space.

2.3.6 Warped Cartesian Grid / Model Construction

The model at the most fundamental level is a series of grid nodes. These nodes define the attributes of the model at specified locations. Four nodes are required to construct a tetrahedral model cell. Eight grid nodes are required to construct a basic block of the model. This block of eight nodes is subdivided into five tetrahedral cells using different combinations of the grid nodes. In order to create a seamless model, the faces of adjacent blocks must connect. For this we require two versions of the basic building block: the standard configuration and its mirror opposite (Figure 17).

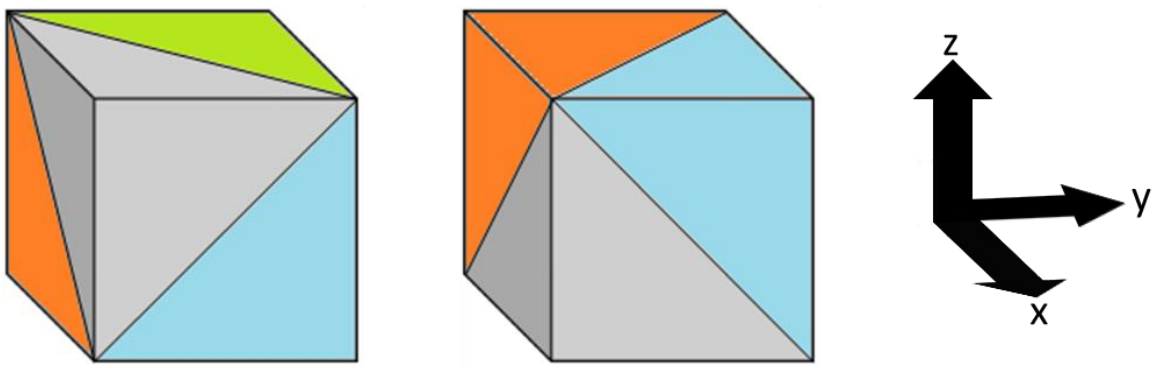

Figure 17 – Basic building blocks consisting of four outer tetrahedra and one inner: standard (left), mirrored (right). The outer tetra configurations are ordered orange, green, blue, gray.

The outer tetrahedra for each building block are built sequentially (Figure 17) to facilitate simple linking procedures. Each of the four outer tetrahedra have three external faces (normals directed away from center). These faces are perpendicular to the x, y, and z axes which we use to identify them i.e. face B is perpendicular to the y-axis, face C is perpendicular to the x-axis, and face D is perpendicular to the z-axis. Face A has a normal directed toward the interior of the block and is used to connect with the internal tetrahedron.

The linking procedure uses the knowledge of the sequentially built blocks and the face directions to connect adjacent blocks. As an example, to link the adjacent blocks seen in Figure 17 we must connect the faces perpendicular to the y-axis. Thus we connect the B faces of the green and blue tetrahedron (left) with the adjacent B faces of the orange and gray (right). Similar linking procedures are done for the x and z axes until we have our full earth model comprised of these basic building blocks (Figure 18).

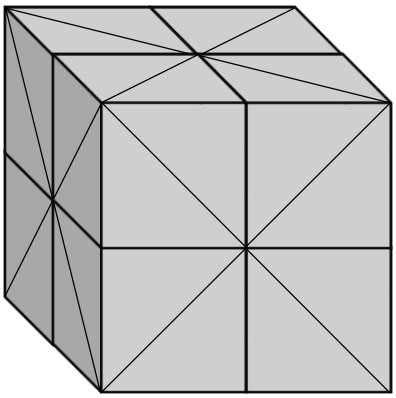

Figure 18 – Example model constructed with basic building blocks.

The grid nodes used to construct the model are indexed in a Cartesian grid fashion (Figure 19). The position of the grid nodes in world space are not constrained to their indexing which results in a warped Cartesian grid. In the figure below a 2-D Cartesian grid is warped in order to simulate a pinch. The indexing remains the same, but we are able to model lateral variations by changing spatial locations of the grid nodes (Figure 19 right).

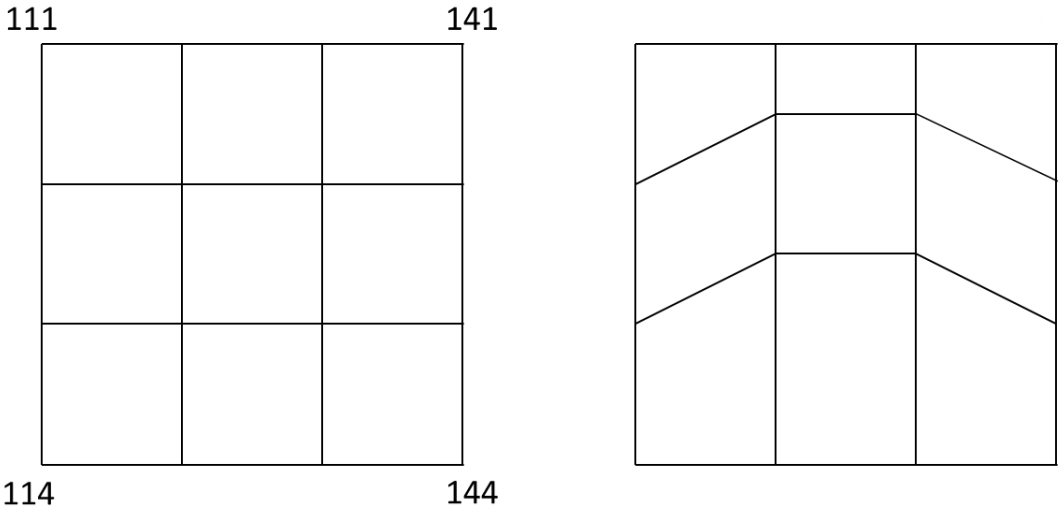

Figure 19 – 2-D Cartesian grid (left) and a warped Cartesian grid (right). Both consist of the same grid nodes (same indexing) but the nodes are at different locations to simulate a pinch in the right scenario.

2.4 Simulation Results

The amplitude ratio P/Lg is a common method of discrimination between an earthquake or explosion event. An explosion is an isotropic emission of compressional energy (P waves) whereas an earthquake source is a slip on fault plane resulting in a quadrupole radiation pattern consisting of both compressional and shear energy. As explosions are not sources of shear energy, the corresponding P/Lg ration will be much larger for explosions. Lateral variations in the crust can block the Lg phase altering the P/Lg ratio, reducing its effectiveness as a discriminant. Using the tools described in previous sections, we construct two earth models to demonstrate the effect of lateral variation in crustal thickness to the Lg phase.

An overly simplified earth model consisting of a 30 km crust, 10 km Moho, and 110 km upper mantle region was constructed as a reference model. An earthquake source radiated two million phonons throughout the model and the resultant energy envelope can be seen in Figure 20. A second model was constructed with a crustal pinch (similar to Figure 19) consisting of a 15 km crust at the maximum pinch. This type of crustal pinch might exist, for example, as a short segment oceanic crust separating two pieces of continental crust. The same earthquake source radiating the same number of phonons (same energy) resulted in a noticeable reduction in the Lg phase (Figure 20). Note that the multiple peaks or scalloping in the synthetics is a result of the Pg and Lg consisting of a series of multiply reflected waves between the surface and Moho. This scalloping tends to be smeared out and disappears as increased scattering by small scale heterogeneities are added to the simulation.

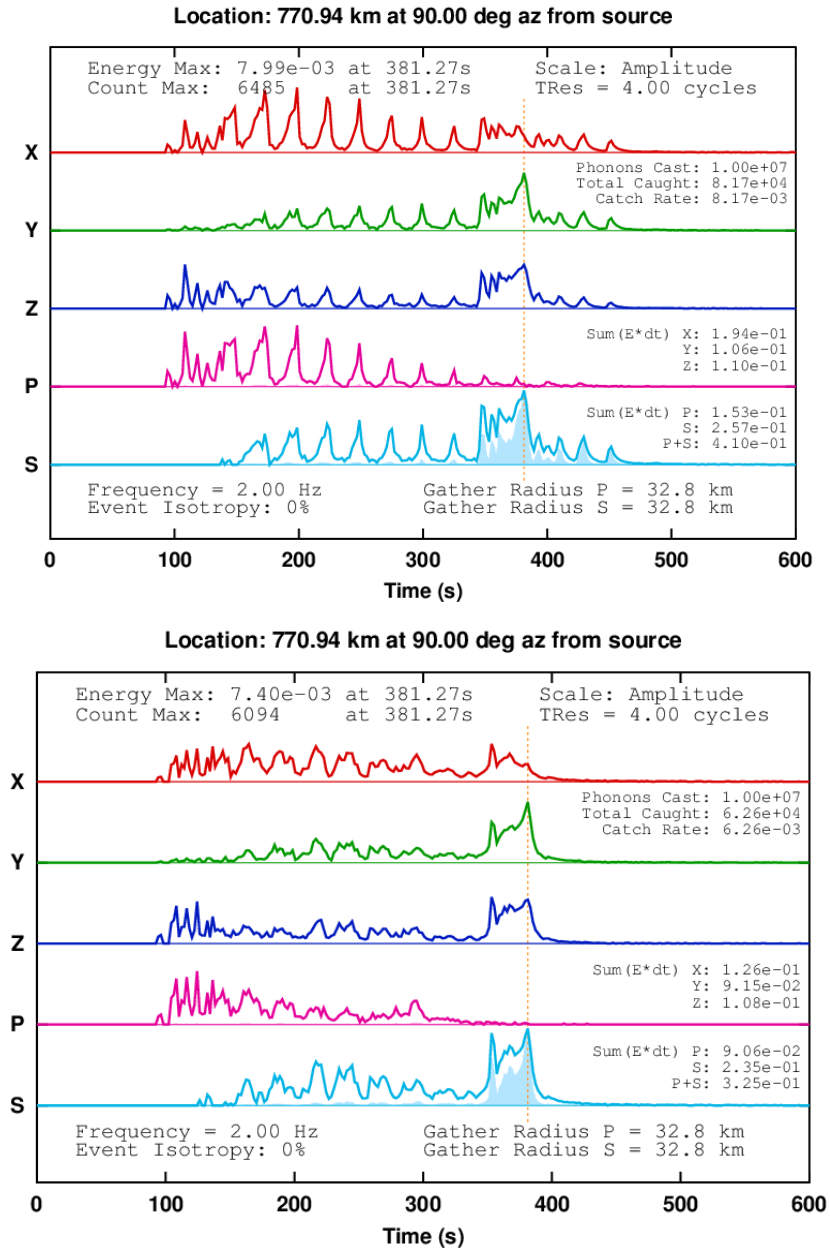

Figure 20—(Top) reference model. (Bottom) pinch model. The energy max (corresponding to the Lg phase) is noticeably diminished in the pinched model.

Below are two frames from post-process videos using the reference model and pinched model described above. These videos give a snap shot of a phonon's position and phase at an instant in time. The first (reference) shows the full Lg phase trapped between the crust and mantle. In the pinched model a large portion of phonons transition into the upper mantle, decreasing the Lg energy in our envelopes.

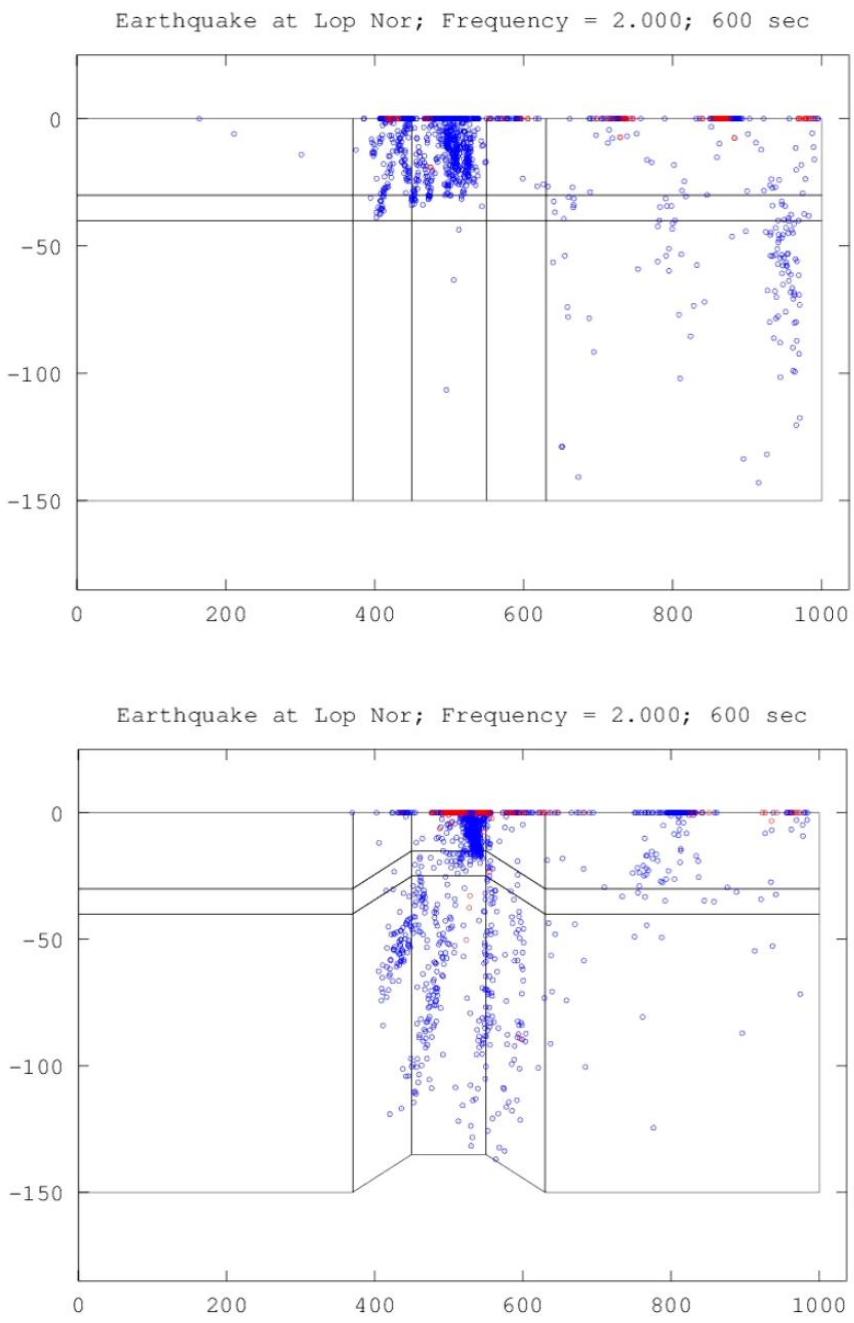

Figure 21 –Snapshot of phonon propagation in our simplified models. (Top) reference model shows large Lg phase trapped between crust and mantle. (Bot) pinched model shows Lg transitioning into upper mantle (Lg blockage).

2.5 Conclusion

Starting from the equation of motion for a continuum it was shown that (at high frequencies) rays are a good approximation for the motion of elastic energy. Given linear gradients, rays follow circular paths that we model using tetrahedral cells. The tetrahedral cells also provide the ability to model lateral variations in earth structure, which are concentrated in the crust and upper mantle. Seismic waves at regional distances (<1000 km) are very sensitive to these variations. Using a warped Cartesian grid and tetrahedral models cells, a synthetic earth model containing lateral variations can be constructed. A model with lateral variations has the potential of emulating the blockage of Lg as seen in the earth. The crustal pinch example seen above, though a simplistic model, shows the capability of this technique to model Lg blockage due to variations in crustal thickness.

2.6 References

Aki, K. and Richards, P.G. (1980), *Quantitative Seismology, Theory and Methods, Vol. I and II*.

Cerveny, V. (2001), *Seismic Ray Theory*.

Cormier, V.F., 2014, *Full waveform modeling of high frequency regional phases for optimization of regional monitoring*, proposal submitted to DOE/NNSA/AFRL BAA solicitation number BAA-RVKV-2014-001, Nuclear Explosion Monitoring.

Kennet, B. L. N. "Lg Waves and Structural Boundaries." *Bulletin of the Seismological Society of America* 76.4 (1986): 1133-1141.

Lay, Thorne, and Terry C. Wallace. *Modern Global Seismology*. San Diego: Academic, 1995.

Menke, W., *Raytrace3d*, IRIS software repository:

http://www.iris.edu/pub/programs/sel/unix/raytrace3d.tar

Sanborn, C.J. (2015). *Radiative3D*: http://rainbow.phys.uconn.edu/geowiki/Radiative3D.

Sato H.,Fehler M.C., *Seismic Wave Propagation and Scattering in the Heterogenous Earth*, (1998), Springer-Verlag, New York.

Shearer, P. M. and Earle, P. S. (2004), *The global short-period wavefield modelled with a Monte Carlo seismic phonon method*. Geophysical Journal International, 158: 1103–1117.

Van Der Hilst, R., *12.510 Introduction to Seismology*, Spring 2008. (Massachusetts Institute of Technology: MIT OpenCourseWare), http://ocw.mit.edu (Accessed July 24, 2015). License: Creative Commons BY-NC-SA

Walter, W.R., Matzel, E., Pasyanos, M.E., Harris, D.B., Gok, R., Ford, S.R. (2007). *Empirical observations of earthquake-explosion discrimination using P/S ratios and implications for the sources of explosion S-waves*, 29th Monitoring Research Review: Ground-based Nuclear Explosion Technologies, report of contract no. W-7405-ENG-48, 2007.